

# RSC Advances



This is an *Accepted Manuscript*, which has been through the Royal Society of Chemistry peer review process and has been accepted for publication.

*Accepted Manuscripts* are published online shortly after acceptance, before technical editing, formatting and proof reading. Using this free service, authors can make their results available to the community, in citable form, before we publish the edited article. This *Accepted Manuscript* will be replaced by the edited, formatted and paginated article as soon as this is available.

You can find more information about *Accepted Manuscripts* in the [Information for Authors](#).

Please note that technical editing may introduce minor changes to the text and/or graphics, which may alter content. The journal's standard [Terms & Conditions](#) and the [Ethical guidelines](#) still apply. In no event shall the Royal Society of Chemistry be held responsible for any errors or omissions in this *Accepted Manuscript* or any consequences arising from the use of any information it contains.



## A cylindrical magnetically-actuated drug delivery device proposed for minimally invasive treatment of prostate cancer

P. Zachkani,<sup>a</sup> J. K. Jackson,<sup>b</sup> F. N. Pirmoradi,<sup>c</sup> and M. Chiao\*<sup>a</sup>

Received 00th January 20xx,  
Accepted 00th January 20xx

DOI: 10.1039/x0xx00000x

www.rsc.org/

A cylindrically shaped magnetically-actuated MEMS (Microelectromechanical Systems) drug delivery device for localized prostate cancer treatment is proposed in this work. The device is designed for implantation through a gauge 12 needle for minimally invasive procedures. The drug delivery device consists of a drug reservoir, a PDMS (polydimethylsiloxane) membrane, a magnetic block and a housing. Under external magnetic fields, the movement of the magnetic block deflects the membrane and discharges the drug through an aperture and into the housing. The housing has a large opening which allows the released drug to diffuse to the surrounding tissues while it prevents the tissues from touching the membrane. On-demand drug release with consistent release rates and device implantation using a needle into ex vivo porcine bladder tissue are demonstrated.

### Introduction

Despite the declining mortality rate in developed countries from prostate cancer, the disease remains a major global health problem as the sixth leading cause of cancer deaths in men.<sup>1</sup> Current methods for treating prostate cancer depend on the stage of the disease and the condition of the patient. For early-stage localized prostate cancer, radical prostatectomy (RP) and radiation therapy (RT) are the primary choices of treatment.<sup>2</sup> New tumor ablation treatments for localized prostate cancer such as HIFU (High-Intensity Focused Ultrasound) brachytherapy and cryosurgery are also emerging as alternatives.<sup>3</sup>

Most prostate cancer treatments have the chance of associated side effects including incontinence, bowel dysfunction and impotence.<sup>4-6</sup> Many patients receive hormone ablation therapy which successfully reduces tumor size to facilitate RP or RT methods but all patients develop resistance to this treatment.<sup>7</sup>

Systemic chemotherapy using docetaxel is a standard treatment for patients with metastatic cancer but it has also been used for localized treatment. In systemic drug administration, the plasma drug concentration needs to be maintained within a defined therapeutic range for a certain time period. However, injections or slow infusions are not

suited to providing these drug regimes. While a high initial concentration of drug may lead to systemic toxicity, a lower concentration of drug later on may not be therapeutically effective. Taxane-based drugs such as docetaxel have narrow therapeutic windows and they are rapidly depleted from the blood after administration. Therefore large fluctuations in the drug concentration in blood, may increase the chance of toxicity or reduce the efficacy of drug therapy.<sup>8,9</sup> Localized drug delivery, on the other hand, is capable of providing localized and controlled drug delivery, which may maintain an effective concentration of drug at the local disease site and hence, reduce the chance of systemic toxicity and adverse side effects.

Generally, many drug delivery devices have been proposed for the local treatment of disease. Passive drug delivery implants release drugs at predetermined rates by osmotic pressure,<sup>10</sup> a porous membrane,<sup>11</sup> polymer degradation<sup>12</sup> or a change in their surroundings such as pH or temperature change<sup>13</sup> with very limited or no dosing flexibility (i.e. no control over the rate and time of release).

One of the advantages of on-demand drug delivery is that drug release can be switched on and off to suit a proposed treatment regimen but may be later adjusted if a relevant change in dosing is required as a result of a sudden and unexpected change in the condition of the patient.<sup>14</sup> An ideal drug delivery device should also be able to adjust the drug release rate. Such devices may increase the efficacy of drug therapy since they can provide a specific release profile tailored to each patient's unique physiology. MEMS-based on-demand drug delivery devices can enable complex dosing schedules, deliver a cocktail of drugs and maintain drug stability inside their reservoirs for extended periods.<sup>15</sup>

Previously, drug release from a MEMS drug delivery device that consisted of a drug reservoir with channels and valves was

<sup>a</sup> Department of Mechanical Engineering, The University of British Columbia, Vancouver, BC, Canada. \*E-mail: muchiao@mech.ubc.ca

<sup>b</sup> Department of Pharmaceutical Sciences, University of British Columbia, Vancouver, BC, Canada.

<sup>c</sup> Palo Alto Research Center, Palo Alto, CA, USA.

† Electronic Supplementary Information (ESI) available: Fabrication process of the 3D-printed device, magnetic field strength of the NdFeB permanent magnet, magnetization of the magnetic film and detailed description of release and mixing time. See DOI: 10.1039/x0xx00000x

achieved by electronically opening the seals or valves of the reservoir.<sup>16,17</sup> Electrochemical and electrothermal opening of thin film reservoir seals was demonstrated by Santini et al.<sup>18-22</sup> Micropumps with diaphragms have also been proposed for drug delivery. Lo et al. developed a manually actuated drug delivery pump for treatment of ocular diseases.<sup>23</sup> Li et al. proposed an electrochemically actuated device with a refillable drug reservoir and a one-way Parylene check-valve.<sup>24</sup> Other micropumps with shape memory alloy or piezoelectric actuation have also been developed.<sup>25</sup> Although most of these active drug delivery devices can precisely control the time of release and drug dosage, they need a power source and therefore, the size of the battery, or wireless inductive power module would dominate the overall device size.

One way to overcome this challenge is to eliminate the on-board power source from the device. Many material-based systems in which the release mechanism is triggered by a laser, near IR light, visual light or ultrasound have been proposed.<sup>26</sup> On-demand<sup>TM</sup> therapeutics has developed a laser-activated device for the treatment of ocular diseases.<sup>10</sup> The device has multiple hermetically sealed reservoirs loaded with drugs and it is implanted inside the eye with an intravitreal injection. When on-demand dosing is required, an opening is created in one of the reservoirs using a laser beam. Additional dosing can take place by puncturing the seals of other reservoirs. This battery-less device may control release kinetics but it should only be implanted in the eye where it can be accessed by a laser beam.

Magnetic actuation of drug delivery micro-pump systems may be another solution for battery-less devices.<sup>25,27-29</sup> However previous devices were too large for minimally invasive surgical procedures and would need large magnetic field gradients to provide magnetic actuation.

This paper reports a new magnetic drug delivery device with a cylindrical geometry and a size that can be implanted through a needle with minimally-invasive procedures, similar to a brachytherapy<sup>30</sup> (a procedure to implant radioactive beads into prostate tissue). The device has an improved actuation mechanism that enables actuating the device at longer distances between the magnet and the device than was reported previously.<sup>27</sup>

## Design

The device and the working principle are schematically illustrated in Fig. 1. As shown in Fig. 1, a rectangular magnetic block is made by sandwiching a layer of magnetic nanoparticles between PDMS layers. The block is bonded to a pure PDMS membrane with an aperture ( $100 \times 100 \mu\text{m}^2$ ). The device also consists of a microreservoir and housing. The main role of the housing is to prevent biological tissues from coming into contact with the thin and sensitive membrane.

When the magnetic block is placed inside a magnetic field, the magnetic translational force exerted on the block can be expressed as:<sup>31</sup>

$$F = \mu_0 v \begin{bmatrix} \frac{\partial}{\partial x} H^T \\ \frac{\partial}{\partial y} H^T \\ \frac{\partial}{\partial z} H^T \end{bmatrix} M \quad (1)$$

where  $F$  is the magnetic translational force,  $\mu_0$  is the permeability of free space,  $v$  is the magnetic block volume,  $H$  is the magnetic field strength and  $M$  is the magnetization of the magnetic block material. We assume that the magnetic field variation in the x-y plane is negligible (Fig. 2). Therefore, the translational force in the z direction is simplified as:

$$F_z = \mu_0 v \frac{\Delta H_z}{t} M_z \quad (2)$$

where  $t$  is the thickness of the magnetic block and  $\Delta H_z = H_{z2} - H_{z1}$  is the difference in the magnetic field strength at the top and bottom surfaces of the magnetic block. The translational force in the z direction pulls the magnetic block towards positive field gradient and consequently deflects the bonded membrane. This deflection discharges the drug solution through the aperture. The drug enters the housing which also serves as a depot from which the released drug can diffuse to the adjacent tissues over time.

Unlike previous magnetic PDMS membranes made by solvent casting methods to incorporate magnetic particles,<sup>32</sup> in this design, the magnetic component is separated from the deflection membrane, so that each part can be manufactured separately and the following improvements can be achieved:

- The amount of magnetic particles in the magnetic block can be increased since particle agglomeration in the magnetic block does not affect membrane-reservoir bonding.
- Thicker magnetic blocks can be manufactured to incorporate more magnetic particles.
- Thinner membranes can be made which require less force for deflection
- A new dry embedding technique can be used to embed uncoated particles with larger magnetization values inside PDMS, eliminating the need for particle coating that is normally required for uniform particle dispersion in the PDMS matrix.

Drug is deposited in the reservoir as a solid drug depot prior to filling the reservoir with bovine serum albumin (BSA) in phosphate buffered saline (PBS pH 7.4) solution (subsequently referred to as BSA solution). This model solution represents the interstitial fluids in the body. After filling the reservoir with BSA solution, a saturated drug solution is formed inside the reservoir some of which is released when the device is actuated. When the magnetic field is removed, the BSA solution surrounding the device refills the reservoir and forms a new saturated solution ready for the next release step. We studied and compared two types of drug, the first model drug, methylene blue (MB), has a high solubility in water (40 g/l) and the second drug, docetaxel (DTX), has a low solubility (7  $\mu\text{g}/\text{ml}$  in water and 71  $\mu\text{g}/\text{ml}$  in 4% w/v BSA solution). Due to the low solubility of DTX in water, we anticipated that the drug release cycle may be repeated with full maintenance of the

DTX concentration, until no more solid DTX is left inside the reservoir.

## Materials and methods

### Fabrication

Two types of devices were fabricated in this work; a larger device (OD = 5 mm, ID = 3 mm, length = 12 mm) made of PDMS and a smaller device (OD = 2 mm, ID = 1 mm, length = 12 mm) made using 3D printing technology (Asiga Pico). The larger PDMS device was used for drug release studies and the smaller 3D-printed device was used for a tissue implantation demonstration through a needle (ID = 2.16 mm). The PDMS device had a membrane thickness of 55  $\mu\text{m}$  and the magnetic block was  $1.5 \times 5 \text{ mm}^2$  with a  $218 \pm 20 \mu\text{m}$  thickness. The housing had a large opening (a 4 mm diameter hole on the PDMS device and a  $1 \times 10 \text{ mm}^2$  narrow opening on the 3D-printed device).

The major fabrication steps of the PDMS device are shown in Fig. 3 and described here: *Step 1:* Two 3D-printed molds were made from Acrylonitrile Butadiene Styrene (ABS); a common thermoplastic material. When put together, the molds create the shape of a drug reservoir. PDMS (Sylgard 184 Silicone Elastomer, Dow Corning Corporation) was prepared with a mixing ratio of 10:1 pre-polymer to cross-linker. One of the molds was filled with PDMS and degassed for 30 minutes. The second mold was placed on top of the PDMS filled mold and pressed on it. The molds were placed in a convection oven at 70 °C for 4 hours. After this time, the molds were detached from each other and the PDMS reservoir was peeled off the molds. *Step 2:* Poly(acrylic acid) (PAA) was used as a sacrificial layer. PAA powder ( $M_w=1800$ , Sigma-Aldrich, ON, Canada) was mixed with distilled water at a 20% w/v concentration. It was mixed and sonicated for 30 minutes and then filtered (4.5  $\mu\text{m}$  pore size, Millipore Corporation, Ma, USA). Two pre-cleaned glass slides were washed with Isopropyl alcohol (IPA) and air dried. The glass slides were treated with air plasma for 75 s to enhance their hydrophilicity. Then, PAA was spun on the glass slides in two steps: 500 rpm for 10 s and 1000 rpm for 30 s. The glass slides were placed on a hot plate at 150 °C for 5 minutes to remove water by evaporation and form the water-soluble sacrificial layer. *Step 3:* The reservoir was then loaded with drug. Firstly, MB was used (Sigma-Aldrich, ON, Canada) as a model drug due to the associated high sensitivity of detection using UV-Vis absorbance spectrometry and clear visual inspection of drug release with eye.<sup>27</sup> A 5% w/v solution of MB in water was deposited in the reservoir and the water content was evaporated. The amount of solid MB in the reservoir may be increased by repeating this cycle. DTX release studies were also carried out using radioactive drug. Tritium-labeled DTX (Moravek Biochemicals Inc., Brea, CA, USA) (50  $\mu\text{Ci}/200 \mu\text{l}$ ) was mixed with unlabeled DTX in a 50% v/v ethanol and 50% v/v dichloromethane (DCM) solution (40 mg/ml) and deposited inside the reservoir similar to MB deposition but after plasma treatment of the reservoir (i.e. *step 5*) to avoid plasma exposure of the drug. *Step 4:* Oxide

nanoparticles  $\text{Fe}_3\text{O}_4$  (Nanostructured and Amorphous materials Inc., Los Alamos, NM, USA) were purchased as a powder and used to make the magnetic block. The powder is 98% w/w pure with an average particle size of 20-30 nm. The magnetic block was made by embedding 2 layers of iron-oxide particles between 3 layers of PDMS. PDMS was spun on a PAA-coated glass slide (500 rpm for 10 s and 1500 rpm for 40 s) and before it was cured, iron-oxide particles were sprinkled on the PDMS layer until the glass slide was fully covered. When the first layer of PDMS was cured, another layer of PDMS was spun on top of this layer with the same spinning parameters and a second layer of magnetic particles was added to increase the weight concentration of magnetic particles in the magnetic film (Note: This method may be repeated several times if a very large magnetic force is required). Each step adds about 100  $\mu\text{m}$  thickness to the magnetic film if the same PDMS pre-polymer to cross-linker ratio (i.e. 10:1) and spinning parameters are used. The final layer of the magnetic film is PDMS to prevent particle leaching from the film in strong magnetic fields. The first layer is also a smooth PDMS layer allowing the magnetic block to bond to the PDMS membrane after surface activation by air plasma. After all layers were formed, the glass slide was immersed in water and the magnetic film was released from the glass slide. A  $1.5 \times 5 \text{ mm}^2$  rectangular piece (referred to as magnetic block) was cut from the magnetic film and a 1 mm diameter hole was punched in the center of the block. *Step 5:* PDMS was spun on a PAA-coated glass slide (500 rpm for 10 s and 1500 rpm for 40 s) and cured in a convection oven at 70 °C for 4 hours. After treating the membrane, drug-loaded reservoir and the magnetic block with air plasma for 75 s at  $\sim 700$  mTorr pressure, the magnetic block was bonded to the membrane and then, the membrane was bonded to the drug-loaded reservoir. The glass slide was immersed in water until the device was released. *Step 6:* The aperture was created by laser ablation using a Nd:YAG laser (Quicklaze, New Wave Research, Sunnyvale, CA). Green laser (532 nm wavelength) with the properties 0.6 mJ (100% high), laser pulses at 35 Hz and a scanning speed of 10  $\mu\text{m}/\text{s}$  was used. *Step 7:* The housing was created with the same procedure as the reservoir (steps 1 and 2). A 4 mm diameter hole was punched into the housing. The reservoir and the housing were treated with air plasma for 75 s at 700 mTorr air pressure and then bonded together. The fabricated device is shown in Fig. 4.

The hydrophobic nature of PDMS inhibits the initial filling of the device with BSA solution. The device was immersed in a glass vial with a 4% w/v aseptically filtered solution of BSA in PBS and then inside a vacuum chamber to force the solution into the reservoir. This enhanced the hydrophilicity of the membrane and the reservoir and enabled complete filling of the reservoir with BSA solution. The device was then placed in a 37 °C oven overnight to incubate. No bubbles were observed inside the reservoir after this step.

The 3D-printed device was made by a similar fabrication process and the steps can be found in the Supplementary Information.†

### Magnetic force and membrane deflection

The magnetic field was created by a cylindrical NdFeB permanent magnet (K&J Magnetics, Pipersville, PA, USA) with a diameter of 0.5 in and a length of 0.75 in. The magnetic field of the permanent magnet was measured as a function of distance from the surface of the magnet with a Bell Gausmeter (Sypris Test & Measurement, FL, USA) and the data is shown in the Supplementary Information.† We used a superconductive quantum interface device (SQUID) (Quantum Design, CA, USA) to measure the magnetic moment of the magnetic film (emu) versus the applied magnetic field (Oe) and the data is shown in the supplementary information.† Assuming that the magnetic film was in the x-y plane, the magnetic field was applied in z direction (perpendicular to the magnetic film) and the magnetism was also measured in that direction (i.e.  $M_z$ ). Magnetization of the sample was measured at two different temperatures; room temperature (25 °C) and body temperature (37 °C), to account for the differences between the laboratory conditions and when the device is implanted in the prostate. The measured values of  $M_z$  at these two temperatures were very close and therefore, we used the magnetization values at 37 °C for all of the calculations. The units were converted into SI units using the density of the magnetic film. A stereo microscope (Olympus, MA, USA) was used to capture images from the magnetic block. The dimensions of the magnetic block were measured by the ImageJ image processing tool. The density of the magnetic block was obtained by dividing the measured weight of three different samples by their volume and was equal to 1.960 ± 0.066 g/cm<sup>3</sup>.

Membrane deflection was measured under various magnetic fields. The PDMS device was fixed on a height-adjustable stage. The permanent magnet was placed on a magnet holder and screwed to a vertical microstage (Melles Griot, NY, USA). A stereo microscope (Olympus, MA, USA) was aligned perpendicular to the axis of the magnet and parallel to the membrane. The distance between the magnetic block and the magnet and the corresponding deflection was measured by image processing using ImageJ software.

### Actuation setup

A permanent magnet (K&J Magnetics) was positioned on a computer-controlled motorized stage (an Atmega328 microcontroller on the Arduino Duemilanove board, by Arduino®, Italy). A device was placed in a petri dish and then on a height-adjustable stage above the magnet. The motorized magnet could move back and forth underneath the device. All distances were measured from the surface of the magnet to the magnetic block on the membrane. The petri dish was filled with 10 mL of 1% w/v BSA in PBS solution. At this point the entire device was submerged under the solution. The height of the stage was adjusted so that the magnetic field at the location of the magnetic block was in the desired range.

An actuation interval consisted of 5 consecutive actuation cycles and each cycle consisted of two time constants; (a) *release time* which we define as the minimum time required

for the release of the maximum volume of the discharged solution under a specific magnetic field in a single actuation and (b) *mixing time*, defined as the minimum time required for the concentration of the pumped-in solution to return to its saturation limit after the magnetic field is removed. The detailed description for calculating release time and mixing time can be found in the Supplementary Information.† After each actuation interval, the solution was stirred and the concentration of the released MB in the BSA solution was measured by UV-Vis spectrophotometry at a wavelength of 660 nm (50 BIO, Varian Medical Systems Inc., Palo Alto, CA, USA). For DTX release, after stirring the solution, three samples with different volumes (100, 200 and 400 µL) were collected from the solution. Each one was mixed with 5 mL of Cytoscint liquid scintillation fluid (Fisher Scientific, Fair Lawn, NJ, USA) and analyzed using a LS 6500 series, multipurpose scintillation counter (Beckman Coulter Inc., Brea, CA, USA). A standard curve that relates the radioactivity in DPM (disintegrations per minute) value to the amount of DTX was obtained by measuring different known concentrations of DTX. Then, the total amount of the released DTX was calculated based on the average DPM values of the three collected samples and converted to the amount of released DTX using the standard curve.

### Cell viability

Human prostate cancer cells (PC3) were grown in DMEM media supplemented with 10% fetal bovine serum and 5% penicillin/streptomycin. Cells were plated in 96 well plates using 1200 cells per well. After one day, the cells were approximately 15% confluent. The drug solution collected from a PDMS device actuation (25 consecutive actuation intervals in a 135.7 mT magnetic field) was measured for docetaxel and found to have a theoretical amount of 6 µg/ml. This solution was diluted down in cell media to 600 ng/ml as a high drug concentration and then serially diluted to low nanogram per mL levels in media. Cells were incubated with 200 µl of each drug solution (n=6 per drug concentration) for 2 days. The media was then removed and cell viability was determined using a nonradioactive cell proliferation MTS assay (Promega, WI, USA) which monitors cellular activity by the mitochondrial conversion of tetrazolium to formazan at 490 nm using a plate reader.

### Tissue implantation

The possibility of implantation through a needle and device operation inside the tissue was investigated by a qualitative *ex vivo* study using porcine bladder tissue. Porcine bladder tissue (thickness approximately 5mm) was sliced into small pieces. Tissue slices were fresh (less than 4 hours from sacrifice) and kept inside a physiological solution (Tyrode's buffer pH = 7.4). A two inch long gauge 12 (ID = 2.16 mm, OD = 2.77 mm) reusable blunt-tip dispensing needle (McMaster-Carr, Aurora, OH, USA) was used to implant the devices into the tissue. The tissue was first pierced with a sharp-tip hypodermic needle

followed by the insertion of blunt-tip needles for device implantation.

For DTX release experiment inside the tissue, a small docetaxel loaded device was inserted into the tissue. The tissue was bathed in Tyrode's buffer and actuated for a number of times. The device was then removed and excess liquid was removed from the tissue. The tissue was then dissolved in tissue solubilizer (Solvabal, Perkin Elmer, USA) overnight and counted for radioactivity. The amount of docetaxel in the tissue was then determined using a calibration graph of known amounts of radiolabelled docetaxel against radioactive counts.

## Results and discussion

### Force and deflection

The saturation magnetization of the magnetic block ( $M_s$ ) is 35.4 emu/g using a 40 kOe magnetic field. The typical magnetization of the particles is 63 emu/g (factory data). Assuming that PDMS has a negligible contribution to the magnetization of the composite, the weight percentage of the magnetic content inside the magnetic block is 56.2%. Compared to solvent casting methods, previously fabricated magnetic PDMS composite had a maximum 32% w/w of magnetic content using coated iron-oxide particles.<sup>32</sup> Therefore the new fabrication technique enables the creation of a magnetic composite that generates 75% more magnetic force using the same magnetic particles and under the same magnetic field. Moreover, unlike a solvent casting technique, the new fabrication technique embeds layers of dry magnetic particles inside PDMS and therefore it does not require particle coating. The absence of surfactant means there would be more room for magnetic content in a given volume of particles (98% w/w iron-oxide content in the particles used in this study compared to 80% w/w iron-oxide content in the particles used in the previously fabricated PDMS composite from our group<sup>32</sup>), resulting in a further increase in the magnitude of a magnetic force.

In the previously fabricated drug delivery device from our team<sup>14</sup> where a magnetic PDMS membrane was created by uniform dispersion of magnetic particles in the PDMS matrix using solvent-casting techniques, there was a trade-off between the degree of magnetic force and deflection because magnetic PDMS generated force and deflection simultaneously. A large magnetic force could be generated by increasing the weight concentration of magnetic particles in the PDMS, but this could have led to particle agglomeration and therefore a non-uniform thickness membrane incapable of making a leakage-free seal with the reservoir. Therefore, the only way to increase the amount of magnetic force was to increase the thickness of the membrane to accommodate more particles. However, a thicker membrane required larger forces for deflection due to the increased bending modulus. As a result of this limitation, large magnetic field gradients were required to provide ample displacements of the membrane. Such strong field gradients only exist in close proximity to an external magnet and therefore, the device could only be

implanted close to the surface of the body where it could be actuated by placing a magnet at a close range. Therefore although that device was a good candidate for the treatment of diabetic retinopathy,<sup>27</sup> where it could be placed at the back of the eye, it was not a good candidate for the treatment of prostate cancer, where the implantation site dictates a longer distance between the magnet and the device. In other words, the new device is designed for prostate implantation and actuation where magnetic actuation may be compromised by the internal location (distance to magnet).

The magnetic force can be calculated from (2). The calculated magnetic forces were used as body loads on a magnetic block in a COMSOL model to simulate membrane deflection. The elastic modulus for Sylgard 184 PDMS with a mixing ratio of 10:1 pre-polymer to cross-linker has been previously reported at 1.8 MPa.<sup>34,35</sup> PDMS Poisson's ratio was reported at 0.5 in the literature.<sup>36,37</sup> In our simulations we used the value 0.45 for Poisson's ratio.<sup>38</sup> Simulated and experimental membrane deflection results are demonstrated in Fig. 5.

Further simulations showed that for a device with a constant diameter, the thickness of the walls have a direct impact on the deflection of the membrane. As the thickness of the walls decrease, the unclamped membrane area increases which facilitates larger deformations under the same magnetic field. However, from a fabrication point of view, thin-wall devices are harder to make and they are prone to wall deformations under physical loads. This consideration is especially important for the 3D-printed devices, which could experience unknown physical loads after implantation.

### MB controlled release

MB was used as a pilot model drug to study release from the device under magnetic actuation. MB has a very high solubility in water (40 g/L) so it was expected that the drug would rapidly deplete from the reservoir after a few actuations, resulting in a decline in the amount of released MB following consecutive actuations. In order to avoid this and to make the device's release rate as consistent as possible, MB-loaded devices were actuated in low magnetic fields (32.9 mT), to minimize the amount of released MB and to ensure that solid MB lasted in the device for longer periods.

Fig. 6(a) shows the cumulative release profile of the MB from the device for the period of three days and the average release rate of MB per actuation interval. Each actuation interval consisted of 5 consecutive actuation cycles, and each cycle consisted of a 50 s actuation time and a 200 s relaxation time. The waiting time between each actuation interval was 60 minutes and drug diffusion was also measured during this time and depicted in the cumulative release diagram.

The device had an average MB release rate of  $27.61 \pm 0.79 \mu\text{g}$  per actuation interval in a 32.9 mT magnetic field. The small standard deviation compared to the average release rate highlights the consistency of the released MB rate. The leakage of MB from the aperture (i.e. background diffusion) for the same duration of one actuation interval was  $1.42 \pm 0.16 \mu\text{g}$

which is almost 20 times smaller than the average release rate during the actuation period (Fig. 6(b)).

### DTX controlled release

In contrast to MB, DTX has a very low solubility in water (5  $\mu\text{g/ml}$ ). The drug is used clinically as an antiproliferative agent and is widely used in chemotherapy. The drug is cytotoxic to prostate cancer cells at nanomolar concentrations (approximately 1–100 nM)<sup>39,40</sup> which makes it an ideal drug candidate for this device because even when low amounts of drug are released per cycle and diluted with interstitial fluid outside the device, effective drug concentrations may be achieved locally. The device was actuated in a 135.7 mT magnetic field over a period of 11 days. The cumulative DTX release profile is shown in (Fig. 6(c)). The device went through five actuation intervals per day. The actuation cycle was 50 s release time with a 200 s mixing time. Drug release rates in each actuation interval were averaged from the measured DPM (radioactive disintegrations per minute) values of three samples with different volumes. These values of the samples were always more than 100 times larger than control (background) levels. Moreover, the DPM values of the samples were linearly proportional to the volume of the collected samples, indicating a quantitative level of reliability for the measurements.

The average release rate of DTX in a 135.7 mT magnetic field was  $353 \pm 36$  ng per actuation interval. The amount of released DTX after 11 days was  $\sim 17$   $\mu\text{g}$ , accounting for only 2% of the initial deposited solid DTX in the reservoir. Therefore, a device with 800  $\mu\text{g}$  of deposited DTX should theoretically have enough drug as a depot to release over 1.5 years in a 135.7 mT magnetic field with the same actuation parameters used in this study.

The role of the housing is to prevent tissues from touching the PDMS membrane, however it is important to have a leakage-free seal between the membrane and the reservoir to minimize drug background diffusion. It has been shown that plasma surface activation and bonding techniques can provide effective seals on PDMS surfaces.<sup>41</sup> In this work, we used plasma bonding techniques and the background diffusion of docetaxel was  $4.8 \pm 0.3$  ng for the same duration of one actuation interval (see Fig. 6(c)), well below 353 ng of drug release per actuation interval. We anticipate that the majority of the background diffusion comes from the aperture. Further studies focusing on background diffusion from the device is needed to fully characterize the seal quality.

DTX release rate was also measured under different magnetic fields to investigate the effect of magnetic field on drug release rate. As shown in Fig. 6(d), normalized DTX release rates are in agreement with the normalized displaced volume caused by membrane deflection.

In comparison to the previously fabricated device from our team<sup>27</sup> where the circular membrane geometry maximized the possible membrane deflection and therefore the volume of released drug, we had to compromise the geometry of the membrane described here due to the required shape of the

device. Although the displaced volume is not the maximum volume that can be achieved by the circular membrane area, we still managed to release comparable amounts of drug from this device (same membrane area under the same magnetic fields) due to the improved actuation mechanism.

### Cell viability

Prostate cancer cells responded well to the drug released from the device. Cell death (reduction in cell proliferation or cell viability) began at around 75 ng/ml and then increased strongly up to 600 ng/ml as shown in Fig. 7. These data confirms that the device releases active drug. The antiproliferative activity of docetaxel which is known to occur in the low nanomolar concentration range, is in broad agreement with the results shown here.

### Tissue implantation

Two 3D-printed MB-loaded devices were filled with 4% w/v BSA solution and implanted in two separate bladder tissue slices. After implantation, the tissue slices were washed with Tyrode's solution and placed in a petri dish. The petri dish was filled with Tyrode's solution until the tissue was submerged, then placed on the height-adjustable stage. One of the devices was actuated for 2 hours in a 206.3 mT magnetic field (10s on/10s off cycles). The other device was used as a control with no actuation. After 2 hours, both tissue slices were cut open and inspected for released MB.

Fig. 8(a) shows the implantation of the device with a blunt tip needle (gauge 12). The released MB in the actuated sample and the control sample are shown in Fig. 8(b) and Fig. 8(c) respectively. Qualitatively, the released MB from the actuated device is clearly noticeable while the non-actuated device has no signs of released MB.

Repeated studies demonstrated high levels of docetaxel were released and partitioned into the bladder tissue. However, in order to overcome drug detection sensitivity issues, it was necessary to actuate the device for extended periods (15 minutes). Under such conditions the amount of docetaxel recovered from bladder tissue was 870 ng. The tissue weighed approximately 1 gram and had a volume of approximately 1 ml so this represents a tissue concentration of close to 1  $\mu\text{g/ml}$ . Since docetaxel released from these devices has been shown to be active and to kill human prostate cancer (PC3) cells *in vitro* at 75 ng/ml (Fig. 7), these drug concentrations represent clinically relevant cytotoxic tissue levels using just one 15 minute actuation protocol. Interestingly, the local docetaxel tissue concentrations around the device were probably considerably higher because it was unlikely that the drug would have diffused throughout the entire 1 gram of tissue in 15 minutes. Since the devices will be located close to tumor foci *in vivo* under ultrasound guidance, this feature offers a further likelihood of an effective anticancer action in a clinical setting. It was not possible to measure tissue concentrations as a function of actuation number because at protocols longer than 15 minutes it is likely that the high local docetaxel concentrations around the device inhibit effective docetaxel

pumping due to the generation of a changing drug gradient towards the device. In practice these devices would be used for shorter actuation time periods than 15 minutes to allow effective drug partitioning into the tissue and some diffusion through the surrounding tissue.

There have been some reports of uncured oligomer and long-term immune responses to PDMS surfaces in vivo.<sup>42-44</sup> Such effects were not studied in this work. However, it should be remembered that these membranes are small and thin so the total amount of uncured oligomer in such a small mass of PDMS would likely be very small. Also the proposed location of the implant is close to tumor tissue so that any minor toxicity arising from non-biocompatibility issues would not be problematic considering the fact that the purpose of the device is to release drugs that kill prostate cancer cells. Strategies to improve biocompatibility of PDMS surfaces such as surface modification have been studied extensively.<sup>45,46</sup> One plausible solution may be to combine PDMS with biocompatible hydrogels.<sup>47,48</sup> However, further studies are required to improve the PDMS biocompatibility.

## Conclusion

In this work we have demonstrated the design and fabrication of a magnetically-actuated and minimally-invasive drug delivery device and presented proof-of-concept controlled release studies. The device is capable of providing defined doses of docetaxel. The proposed implantation method of this device is similar to radioactive seed implantation used in brachytherapy, where the convenience of implantation enables the patient to return to his daily activities after a few days while avoiding complications that could have occurred by the alternative invasive surgery. We expect that the fine-tuned and localized dosing of DTX would add to the efficacy of drug therapy. Therefore, this device may be used to complement the active surveillance strategy (i.e. a prostate cancer management strategy for the earliest stages of tumor, in which no treatment is undertaken until signs of cancer progression are observed) in order to treat or slow down cancer progression. After device implantation, the exact position of the device may be mapped by x-ray or ultrasound. Then an electromagnet can be inserted through the patient's rectum and adjacent to his prostate. By adjusting the current passing through the electromagnet, a specific magnetic field gradient can be created at the location of the device and actuate it. Compared with previous devices from our group<sup>14</sup>, the new design and new fabrication technique enabled a magnetic composite with a higher concentration of magnetic particles. This led to an increased magnetic force generated in the same magnetic field compared to the previously fabricated magnetic PDMS composite and enabled the possibility of creating a thinner membrane that can create larger deformations under a given load. These two factors enabled the device to be actuated at a longer distance from the magnet. This, together with the possibility of device implantation through a needle, opens up new minimally-invasive treatment applications by implanting the device deeper inside the body. Moreover, due

to the small size of the device, we anticipate that more than one device can be implanted in a small area such as prostate and deliver a more uniformly distributed drug load to the tissue.

Membrane deflection of the PDMS device was simulated and experimentally verified under various magnetic fields. The device has a consistent release rate of  $353 \pm 36$  ng per actuation interval under a 135.7 mT magnetic field for DTX. Device implantation into porcine bladder tissue through a needle was also demonstrated. After implantation the device operated successfully inside the tissue.

## Acknowledgement

This work has been supported by an NSERC/CIHR CHRP Grant (CHRP 414087-12), Canada Foundation for Innovations and UBC's Institute for Computing, Information and Cognitive Systems (ICICS). We would like to thank Professor H. M. Burt of the UBC's Faculty of Pharmaceutical Sciences for providing us with lab space and equipment. We would also like to thank Prof. D. Leznoff of SFU's Department of Chemistry for the help with the superconducting quantum interface device measurements.

## References

- 1 A. Jemal, F. Bray, M. M. Center, J. Ferlay, E. Ward and D. Forman, *CA-Cancer J. Clin.*, 2011, **61**, 69-90.
- 2 A. J. Roth, M. I. Weinberger and C. J. Nelson, *Future Oncol.*, 2008, **4**, 561-568.
- 3 N. Mottet, P.J. Bastian, J. Bellmunt, R. C. N. van den Bergh, M. Bolla, N. J. van Casteren, P. Cornford, S. Joniau, M. D. Mason, V. Matveev, T. H. van der Kwast, H. van der Poel, C. Rouvière and T. Wiegel, *Guidelines on Prostate Cancer*, European Association of Urology, 2014.
- 4 F. J. Fowler Jr, M. J. Barry, G. Lu-Yao, J. Wasson, A. Roman and J. Wennberg, *Urology*, 1995, **45**, 1007-1015.
- 5 F. J. Fowler Jr., M. J. Barry, G. Lu-Yao, J. Wasson and L. Bin, *J. Clin. Oncol.*, 1996, **14**, 2258-2265.
- 6 National Cancer Institute, *Treatment choices for men with early-stage prostate cancer*, NIH publication, No. 11-4659, 2011.
- 7 S. S. Sridhar, S. J. Freedland, M. E. Gleave, C. Higano, P. Mulders, C. Parker, O. Sartor and F. Saad, *Eur. Urol.*, 2014, **65**, 289-299.
- 8 G. Gaucher, R. H. Marchessault, and J.C. Leroux, *J. Controlled Release*, 2010, **143**, 2-12.
- 9 F. K. Engels, W. J. Loos, J. M. van der Bol, P. de Bruijn, R. H. J. Mathijssen, J. Verweij and R. A. A. Mathot, *Clin. Cancer Res.*, 2011, **17**, 353-362.
- 10 C. L. Stevenson, J. T. Santini Jr. and R. Langer, *Adv. Drug Deliver Rev.*, 2012, **64**, 1590-1602.
- 11 G. Jeon, S. Y. Yang and J. K. Kim, *J. Mater. Chem.*, 2012, **22**, 14814-14834.
- 12 A. Göpferich, *Biomaterials*, 1996, **17**, 103-114.
- 13 R. Yoshida, *Curr. Org. Chem.*, 2005, **9**, 1617-1641.

- 14 F. N. Pirmoradi, J. K. Jackson, H. M. Burt and M. Chiao, *Lab Chip*, 2011, **11**, 2744-2752.
- 15 M. Staples, *Wiley Interdiscip. Rev.: Nanomed. Nanobiotechnol.*, 2010, **2**, 400-417.
- 16 A. C. R. Grayson, R. S. Shawgo, A. M. Johnson, N. T. Flynn, Y. Li, M. J. Cima and R. Langer, *Proc. IEEE*, 2004, **92**, 6-21.
- 17 D. A. LaVan, T. McGuire and R. Langer, *Nat. Biotechnol.*, 2003, **21**, 1184-1191.
- 18 J. T. Santini, M. J. Cima, and R. Langer, *Nature*, 1999, **397**, 335-338.
- 19 J. M. Maloney, S. A. Uhland, B. F. Polito, J. N. F. Sheppard, C. M. Pelta, and J. J. T. Santini, *J. Controlled Release*, 2005, **109**, 244-255.
- 20 J. H. Prescott, S. Lipka, S. Baldwin, N. F. Sheppard, J. M. Maloney, J. Coppeta, B. Yomtov, M. A. Staples, and J. T. Santini, *Nat. Biotechnol.*, 2006, **24**, 437-438.
- 21 D. Ge, X. Tian, R. Qi, S. Huang, J. Mu, S. Hong, S. Ye, X. Zhang, D. Li and W. Shi, *Electrochim. Acta*, 2009, **55**, 271-275.
- 22 N. M. Elman, H. L. Ho Duc and M. J. Cima, *Biomed. Microdevices*, 2009, **11**, 625-631.
- 23 R. Lo, K. Kuwahar, P. Y. Li, S. Saati, R. N. Agrawal, M. S. Humayun and E. Meng, *Biomed. Microdevices*, 2009, **11**, 959-970.
- 24 P. Y. Li, J. Shih, R. Lo, S. Saati, R. Agrawal, M. S. Humayun, Y. C. Tai and E. Meng, *Sens. Actuators, A*, 2008, **143**, 41-48.
- 25 F. Amirouche, Y. Zhou and T. Johnson, *Microsyst. Technol.*, 2009, **15**, 647-666.
- 26 B. P. Timko, T. Dvir, and D. S. Kohane, *Adv. Mater. (Weinheim, Ger.)*, 2010, **22**, 4925-4943.
- 27 F. N. Pirmoradi, J. K. Jackson, H. M. Burt and M. Chiao, *Lab Chip*, 2011, **11**, 3072-3080.
- 28 T. Pan, S. J. McDonald, E. M. Kai and B. Ziaie, *J. Micromech. Microeng.*, 2005, **15**, 1021-1026.
- 29 B. L. Gray, *J. Electrochem. Soc.*, 2014, **161** (2), B3173-B3183.
- 30 A. V. D'Amico, R. Cormack, C. M. Tempany, S. Kumar, G. Topulos, H. M. Kooy and C. N. Coleman, *Int. J. Radiation Oncology Biol. Phys.*, 1998, **42**, 507-515.
- 31 J. J. Abbott, O. Ergeneman, M. P. Kummer, A. M. Hirt, and B. J. Nelson, *IEEE Trans. Robotics*, 2007, **23**, 1247-1252.
- 32 F. N. Pirmoradi, L. Cheng, and M. Chiao, *J. Micromech. Microeng.*, 2010, **20**, 015032.
- 33 F. Khademolhosseini and M. Chiao, *J. Microelectromech. Syst.*, 2013, **22**, 131-139.
- 34 F. Schneider, T. Fellner, J. Wilde and U. Wallrabe, *J. Micromech. Microeng.*, 2007, **18**, 065008.
- 35 K. M. Choi and J. A. Rogers, *J. Am. Chem. Soc.*, 2003, **125**, 4060-4061.
- 36 Y. S. Yu and Y. P. Zhao, *J. Colloid Interface Sci.*, 2009, **332**, 467-476.
- 37 A. Folch, *Introduction to BioMEMS*, CRC Press, 2012.
- 38 V. Studer, G. Hang, A. Pandolfi, M. Ortiz, W. F. Anderson and S. R. Quake, *J. Appl. Phys.*, 2004, **95**, 393-398.
- 39 J. C. Forde, A. S. Perry, K. Brennan, L. M. Martin, M. P. Lawler, T. H. Lynch, D. Hollywood and L. Marignol, *Urol. Oncol-Semin. Ori.*, 2012, **30**, 912-919.
- 40 D. E. Oprea-Lager, I. V. Bijnsdorp, R. J. A. Van Moorselaar, A. J. M. Van Den Eertwegh, O. S. Hoekstra and A. A. Geldof, *Anticancer Res.*, 2013, **33**, 387-392.
- 41 D. C. Duffy, J. C. McDonald, O. J. A. Schueller and G. M. Whitesides, *Anal. Chem.*, 1998, **70**, 4974-4984.
- 42 K. J. Regehr, M. Domenech, J. T. Koepsel, K. C. Carver, S. J. Ellison-Zelski, W. L. Murphy, L. A. Schuler, E. T. Alarid and D. J. Beebe, *Lab Chip*, 2009, **9**(15), 2132-2139.
- 43 K. M. Ainslie and T. A. Desai, *Lab Chip*, 2008, **8**(11), 1864-1878.
- 44 H. Zhang and M. Chiao, *J. Med. Biol. Eng.*, 2015, **35**, 143-155.
- 45 I. Wong and C. M. Ho, *Microfluid. Nanofluid.*, 2009, **7**, 291-306.
- 46 Q. Tu, J. C. Wang, Y. Zhang, R. Liu, W. Liu, L. Ren, S. Shen, J. Xu, L. Zhao and J. Wang, *Rev. Anal. Chem.*, 2012, **31**, 177-192.
- 47 H. Zhang, C. Bian, J. K. Jackson, H. M. Burt and M. Chiao, *Adv. Mater. Interfaces*, 2015, **2**, DOI: 10.1002/admi.201500154.
- 48 H. Zhang, C. Bian, J. K. Jackson, F. Khademolhosseini, H. M. Burt and M. Chiao, *ACS Appl. Mater. Interfaces*, 2014, **6**(12), 9126-9133.

## Figures

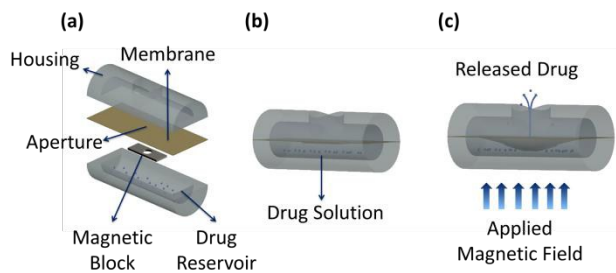


Fig. 1 Conceptual diagram of the proposed minimally-invasive drug delivery device showing (a) device components, (b) device under no magnetic field and (c) actuated device under an applied magnetic field.

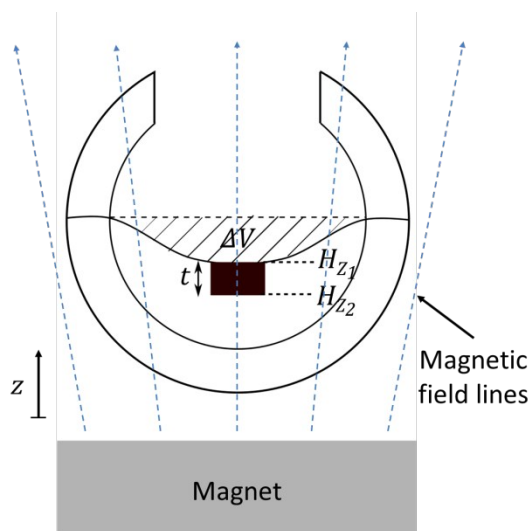


Fig. 2 Schematic illustration of the cross section of a device actuated using a permanent magnet.

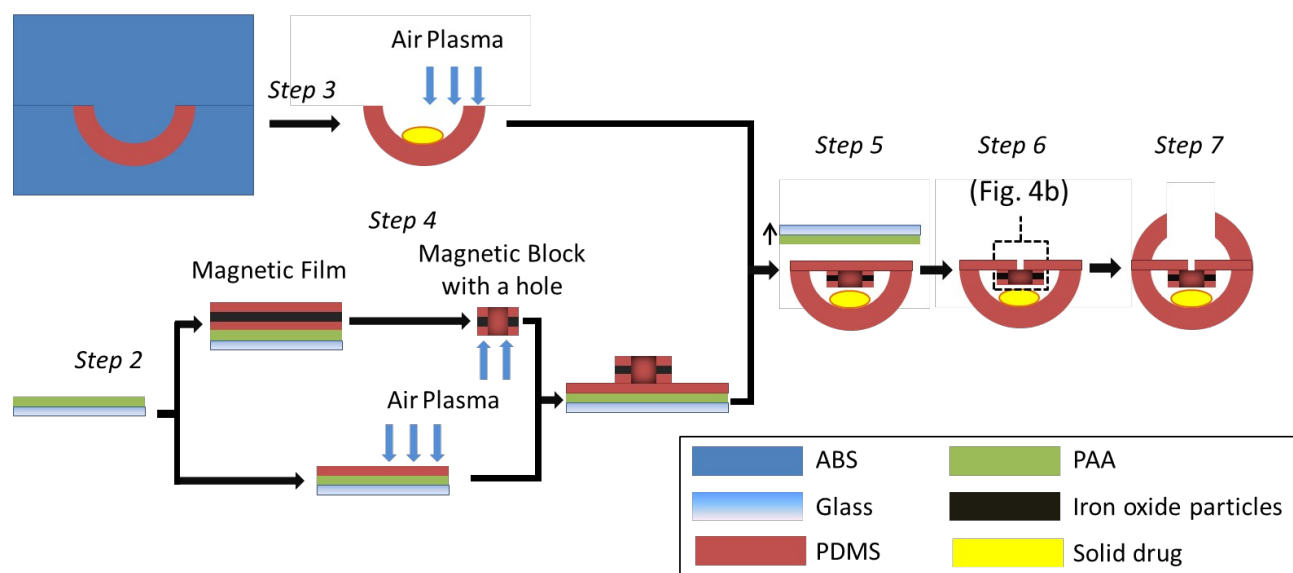


Fig. 3 Fabrication steps of the PDMS device.

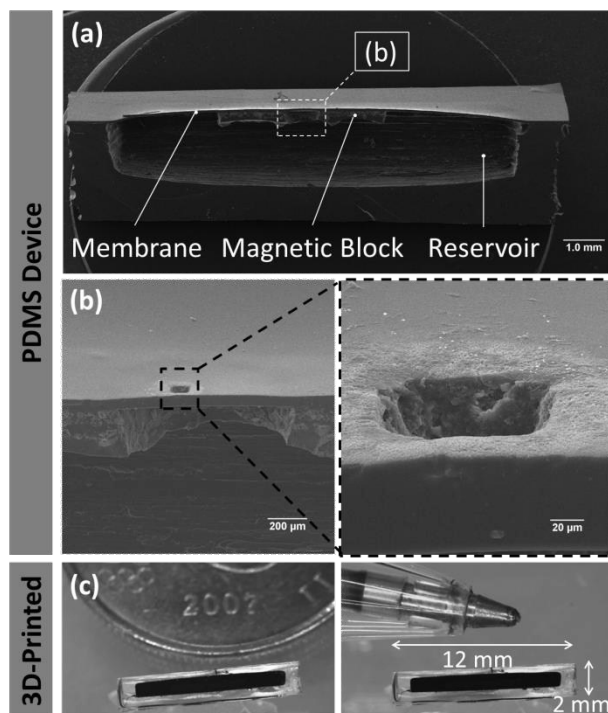


Fig. 4 (a) SEM image of the fabricated PDMS device (without housing), (b) close-up SEM views of the aperture on the membrane and (c) 3D-printed device (without housing).

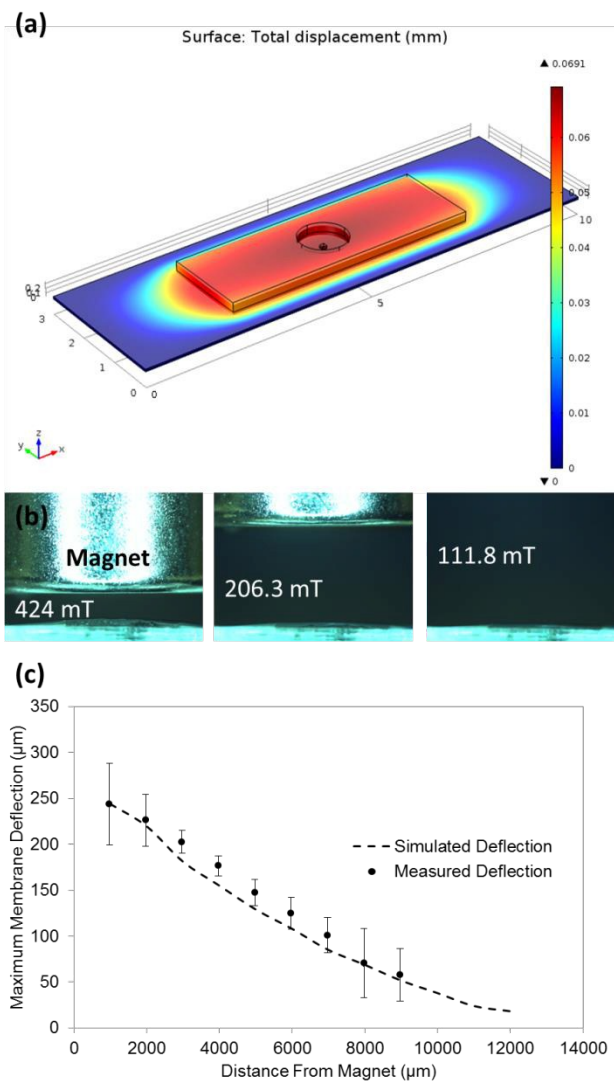


Fig. 5 Deflection of the membrane (a) simulated deflection in a 92.9 mT field, (b) actual deflection in 424 mT, 206.3 mT and 111.8 mT magnetic fields and (c) comparison between simulation and experimental results. The error bars represent one standard deviation from the measured values.

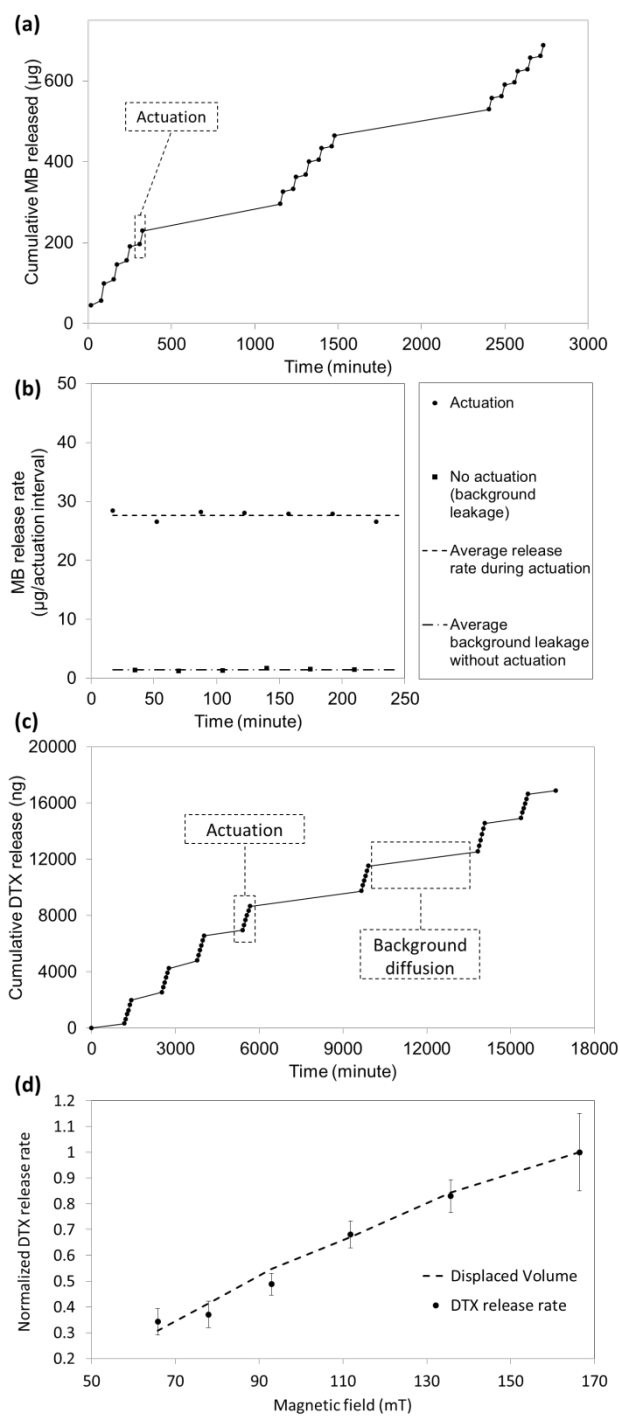


Fig. 6 Controlled release of MB and DTX from the device, (a) cumulative MB release profile over 3 days in a 32.9 mT magnetic field, (b) average MB release rate per actuation interval in a 32.9 mT magnetic field, (c) cumulative DTX release profile over 11 days in a 135.7 mT magnetic field. Background diffusion for the same duration of one actuation interval is measured as  $4.8 \pm 0.3$  ng. (d) the effect of magnetic field strength on DTX release rates.

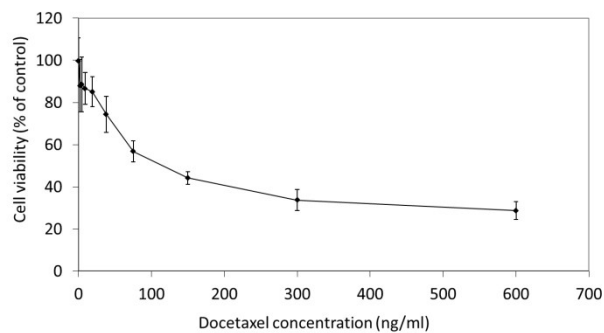


Fig. 7 Viability of prostate PC3 cells after incubation with drug release media from the device.

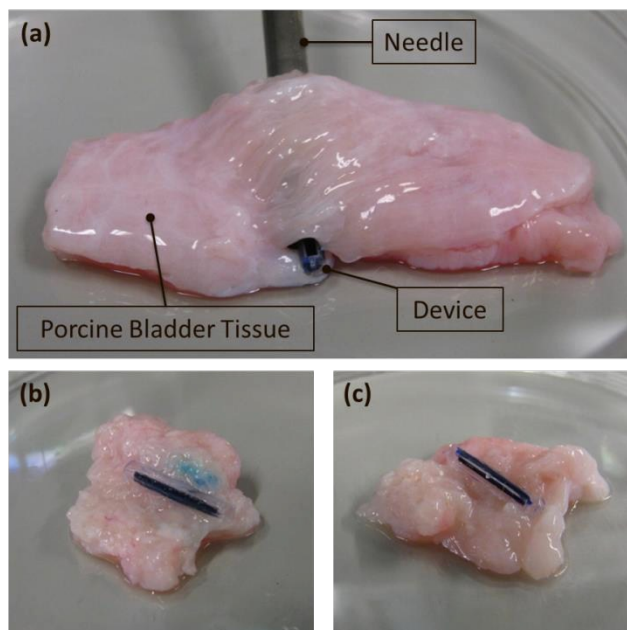


Fig. 8 (a) Device implantation in porcine bladder tissue with a gauge 12 needle, (b) actuated device showing released MB after two hours of actuation in a 206.3 mT magnetic field and (c) control sample with no actuation after two hours.

## Graphical Abstract

A cylindrical magnetically-actuated MEMS drug delivery device, implanted through a needle for localized prostate cancer treatment is proposed.

